Error Characterization for Cloud Microphysics Probes Using Laboratory Calibration and In-Situ Analysis

Thesis Research Proposal

Spencer Faber

University of Wyoming, Atmospheric Science Department
Laramie, Wyoming

1. Overview

Characterization of clouds and the ability to accurately model a range of microphysical processes, including droplet activation, growth, and precipitation formation, is crucial to improving our ability to predict everything from localized precipitation to global cloud albedo. A more thorough understanding of these processes is required despite many years of focused work and rapid advances in computer modeling and in-situ probe capacities. Continued improvement of cloud, weather, and climate models requires a detailed understanding of how processes influence deviations from adiabatically-predicted values (Morrison et al. 2014). Investigations are complicated by many factors including the fact that relevant processes are modified by complex feedback mechanisms and occur on temporal and spatial scales which span orders of magnitude. Further challenges are presented by the incomplete characterization of probe limitations.

The use of cloud droplet size distributions (DSDs) is nearly ubiquitous in cloud microphysical studies because they provide key insight regarding droplet formation, precipitation initiation, and feedbacks through dynamic processes (Lamb and Verlinde 2011). Furthermore, several distribution statistics (for example kurtosis, skewedness, and measures of bi-modality) are characteristic to specific cloud properties and processes. Distributions composed of small diameter droplets are especially useful for studies focusing on droplet growth through condensation and initial precipitation formation. Clouds composed of newly-activated droplets show narrow DSDs of small mean diameter because the rate of diameter change through condensation is inversely proportional to droplet diameter. Growth to precipitation-sized particles by condensation alone would require timescales far longer than are observed, implying the importance of additional processes. One such process, droplet collection and coalescence, widens narrow small droplet distributions to a more disperse bi-modal shape (Lamb and Verlinde 2011). Small droplet distribution widening can in turn lead to positive coalescence feedbacks (due to droplet terminal velocity being proportionally related to diameter squared) which accelerate droplet growth rates (Gunn and Kinzer 1949).

Ice processes further complicate DSD evolutions and precipitation formation studies. The Bergeron process, which is driven by the fact that saturation vapor pressure over ice is less than that over supercooled liquid water, can quickly (with regards to convective cloud lifetime) accelerate ice particle growth. Furthermore, ice particles are subject to interactions with other particles including growth through droplet collection and freezing, aggregational growth, and splintering caused by impacts with other ice particles. Impact splintering can lead to positive ice formation feedbacks by increasing the number of frozen particles.

Dynamic processes including entrainment, mixing, and particle recycling can also affect DSD evolutions (Tölle, 2014). For example, the mixing of entrained sub-saturated air can influence DSD evolution in a number of ways depending (primary) upon the relationship of timescales required to “mix in” entrained air and the characteristic time required to evaporate entrained droplets. At one end of the spectrum, DSDs subject to

mixing timescales much greater than evaporative timescales will exhibit deceased particle counts but show little change in distribution shape. In contrast, if a distribution's evaporative timescale is greater than the entrained air's mixing timescale the droplet distribution will be shifted towards a small mean diameter with little change in droplet counts (Tölle, 2014).

2. Airborne Measurements of Droplet Size Distributions and Water Content

2.1 The Cloud Droplet Probe Forward Scattering Spectrometer

The Droplet Measurement Technologies, Inc. Cloud Droplet Probe (CDP) is a cloud particle counting and sizing instrument commonly used to provide measurements of DSD from aircraft. In essence, the CDP retrieves droplet distributions (of up to 50 μm diameter) using a diode laser and a pair of photodetectors. Particles pass through the laser beam and scatter light which is collected in a 4 - 12 degree arc. Collected light is split and relayed to an unmasked "sizing" photodetector and a rectangularly masked "qualifier" detector. Particles are placed in one of 30 size bins (of 1 μm resolution for particles up to 14 μm diameter or 2 μm resolution for particles with diameters of 14 – 50 μm) according to the sizing detector's pulse amplitude and Mie theory principles (Droplet Measurement Technologies, inc., 2014). The qualifier detector ensures that particles pass through the instrument's designated sample volume which is essential because intensity of collected light is highly dependent on particle position. Several other parameters can be calculated using CDP DSDs including liquid water content (LWC), effective particle diameter, and particle concentration (Droplet Measurement Technologies, inc., 2014). The probe also includes a particle-by-particle (PBP) feature which returns detector pulse amplitudes and particle inter-arrival times (time since last detected particle) for the first 256 counting events within a sample interval. Table 1 outlines the CDP's retrievable parameters.

Table 1. CDP Retrievable Parameters

Parameter	Source
Particle Diameter	Scattered light intensity
Particle Number Concentration	Scattering event counts, sample volume dimensions, aircraft airspeed
Liquid Water Content	Derived from DSD
Effective Diameter	Derived from DSD
Median Volume Diameter	Derived from DSD
Particle-By-Particle Sizing Response†	Scattered light intensity
Particle-By-Particle Inter-Arrival Time†	Clock cycles since last scattering event

†*Particle-by-Particle data are available for the first 256 particles in each sample interval.* (Droplet Measurement Technologies, Inc., 2014)

The CDP operates on principles similar to the Particle Measuring Systems, Inc. Forward Scattering Spectrometer Probe (FSSP) but incorporates several changes including improved circuitry to shorten response times (by extension, eliminating dead-time losses), a unimodal laser intended to decrease variations in beam intensity, and an updated qualifier detector designed to more accurately determine when particles are within the sample volume (Lance et al., 2010).

2.2 The Nevzorov Hotwire Probe

The Nevzorov is among the latest generation of hotwire probes capable of retrieving both bulk liquid water content and combined liquid/ice water content (LWC, TWC). The Nevzorov has several advantages over other hotwire designs including phase discrimination capability, a freely rotating vane to decrease aircraft orientation bias, and paired collector/reference sensor architecture. Paired sensors simplify calculations of convective heat loss (power consumption due to sources other than particle evaporation), significantly reduce baseline noise, and increase retrieval confidence in low water content environments (Korolev et al. 1998).

Water contents are calculated using the power consumption of two constant-temperature elements; one in the form of a coil intended to collect only liquid particles (LWC collector sensor) and the other shaped as an inverted cone which is designed to capture and sense particles of both phases (TWC collector sensor). Both the LWC and TWC collector sensors are paired with similarly-sized reference sensors positioned so cloud particle impacts are unlikely (therefor reference sensor power consumption is assumed to be caused by convective heat losses only). Figure 1 shows the Nevzorov's general layout including collector and reference sensor locations.

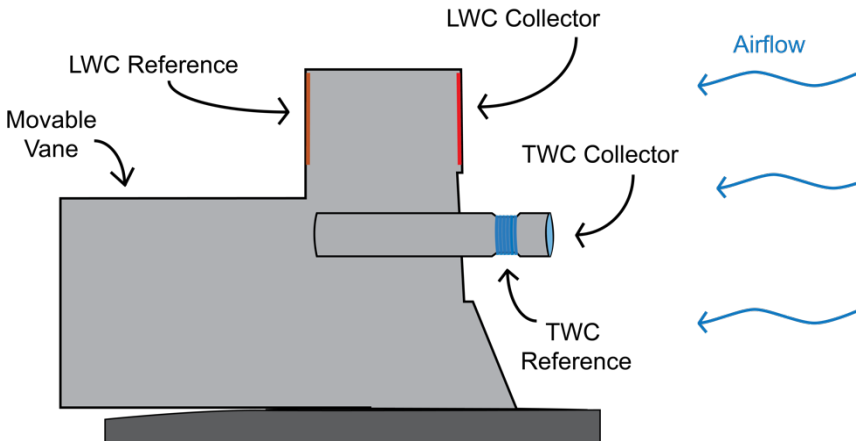

Figure 1. *Schematic of the Nevzorov probe illustrating collector/reference sensor pairing. The vane (vertical light grey structure) is freely rotating to ensure that reference sensors don't experience particle impacts and collector sensor faces remain orthogonal to the airflow.*

Hotwire-sensed LWC holds utility for both model and observationally based studies. Water content is a key parameter in bulk cloud models which, perhaps most importantly, provides a constraint on precipitable water values. Hotwire-sensed LWC is also useful for airborne probe limitation studies because bulk water content values are analogous to a droplet distribution's integrated third moment. Both the Nevzorov and CDP are capable of calculating LWC (the Nevzorov through bulk measurements and the CDP through DSD-derived values) which provides opportunity for probe error assessment studies. Furthermore, Nevzorov and CDP LWC have been shown to be in good agreement in a variety of operating conditions. In-situ analysis preformed by Sulskis (2016) investigated CDP and Nevzorov LWC agreement across various mean particle diameters ranging 5 to 30 μm and particle concentrations ranging 10 to 1500 cm^{-3}. CDP and Nevzorov LWC were within 13% agreement across nearly all diameter and concentration ranges.

3. Significance

3.1 Error Sources Affecting CDP Measurements

The CDP is subject to both significant particle mis-sizing and mis-counting error. Mis-sizing error can be caused by a variety of effects that fall into two overarching categories; sizing response error and coincidence error. Sizing response errors are primarily caused by inhomogeneity in laser beam intensity, Mie theory ambiguities, and optical component mis-alignment. Lance et al. (2010) demonstrated that even minor misalignment can lead to significant particle sizing bias because such imperfections alter light collection angles (and therefor affect the intensity of light impinging on the sizing detector array). The same study found that various sources of sizing response error can skew particle diameter values by 2 μm. Coincidence events are the second overarching category of effects which can contribute to mis-sizing error. A coincidence event occurs when multiple particles are simultaneously within an instrument's beam. Such occurrences can lead to errors in sizing because the additional light scattered by coincident particles can be collected and sensed by the CDP. Coincidence error is more difficult to parameterize than "pure" sizing response error because a variety of factors (including particle concentration and the coincident particles' position and size) can lead to several different outcomes.

Coincidence error can also lead to significant particle counting uncertainty because, at most, a counting event is triggered for only one of the coincident particles. The additional light scattered by coincident particles can also raise digital sizing counts above threshold values and cause none of the coincident particles to be counted. Manufacturer specifications state the CDP is capable of truthfully retrieving DSDs in concentrations of up to 2,000 particles cm^{-3} but studies have shown that coincidence effects can contribute to 27% undercounting error at concentrations as low as 500 particles cm^{-3} (Droplet Measurement Technologies, Inc., 2014, Lance et. al., 2012). The University of Wyoming King Air (UWKA) CDP features a sizing detector pinhole mask

intended to decrease the occurrence of coincidence events. Lance et al. (2012) demonstrated that sizing detector pinhole masks do significantly decrease the impact of coincidence events but an instrument-specific investigation is nonetheless pertinent.

To be clear, sizing response error is considered to be a “single particle” phenomenon which most likely contributes to systematic particle sizing error. In contrast, coincidence error is a concentration dependent event which can lead to both errors in particle counting and sizing. Error introduced by coincidence events is much less predictable because it can lead to different outcomes depending on several factors.

Investigating the nature of sizing response error requires detailed measurements of sample volume dimensions and sizing response truthfulness at discrete positions within the sample volume. Traditional techniques used to calibrate forward scattering spectrometers aren’t suitable for such investigations because they lack the required precision in particle placement and concentration. Furthermore, they use glass microbeads or polystyrene spheres as calibration media; both of which introduce complexities due to their differences in refractive indices (with respect to water) and imprecise particle shape and size. A handful of institutions and instrument manufactures have developed water droplet calibration devices (or “droplet generators”) to improve calibration and better characterize instrument response. These devices are designed to create pure water droplets of repeatable size, velocity, concentration, and placement; attributes which would allow for calibration and uncertainty investigations less affected by refractive index problems and spatial uncertainty.

3.2 Error Sources Affecting Nevzorov Measurements

Bulk measures of LWC and TWC from the Nevzorov can be compromised by various error sources including sensor saturation in high water content environments, non-unity particle collection efficiency, and convective heat losses. It has been found that LWC sensor saturation is significant for droplets with median volume diameters (MVD) greater than 50 μm (Strapp et al. 2003) or LWC greater than 1.3 g m^{-3} (Sulskis 2016). Sulskis’ findings were mainly employed as a threshold value; ranges of actual affected water content measurements vary based on operating conditions. Sensor saturation error is considered to be of secondary concern because the latest design of the UWKA Nevzorov probe features updated circuitry which should minimize power supply bottlenecks.

Convective heat losses (or sensor power consumption due to factors other than particle evaporation) are an airspeed and atmospheric density dependent phenomena that can seriously compromise Nevzorov measurements. Calculations often use a mean convective heat loss approximation and therefor neglect the affect of fluctuations in airspeed and air density. Such approximations can introduce pronounced LWC baseline drift and error on the order of 100%. Figure 2a shows a comparison of LWC calculated with a convective heat loss value that is based on parameterizations of airspeed and air density (black line) and LWC calculated using a fixed mean convective heat loss value

(red line). The red line illustrates the typical character of baseline drift introduced by using such heat loss approximations.

A 1998 study by Korolev et al. investigated LWC sensor collection efficiencies for droplets with volume weighted mean diameters (VMD) of 2 – 25 μm. subsequent work by Schwarzenboeck et al. (2009) expanded LWC efficiency estimates to include droplets of up to 300 μm VMD. The two studies indicate collection efficiency effects are significant for droplet VMD less than 5 μm (due to aerodynamic effects) or greater than 25 μm (due to incomplete evaporation).

Korolev et al.'s 1998 study also examined TWC droplet collection efficiencies for 2 – 25 μm VMD particles and estimated that efficiencies are significantly less than unity for small droplets (~ 3 – 15 μm VMD) but approach values of .9 by 25 μm VDM. Figure 2b shows a CDP droplet distribution for measurements collected during several missions flown during the Convective Precipitation Experiment - Microphysics and Entrainment Dependencies (COPE-MED) campaign. Overlaid collection efficiency estimates (provided by Korolev et al. 1998, Strapp et al. 2003, Schwarzenboeck et al. 2009) show that collection efficiency effects are especially apparent for both LWC/TWC sensor measurements taken in distributions with VMD of 12 μm or less. Estimates of TWC collection efficiencies for droplets as large as 236 μm MVD were later examined in work by Strapp et al. (2003) in which wind tunnel tests supported that TWC efficiencies remain near unity for large droplets. It should be noted that Strap et al. used extrapolated TWC efficiency estimates for 25 - 50 μm VMD droplets (due to equipment limitations). It is reasonable to assume that efficiencies in that range follow a well-behaved pattern but further in-situ analysis is pertinent because estimates of TWC collection efficiency are key for phase discrimination and water content calculations in mixed-phase clouds.

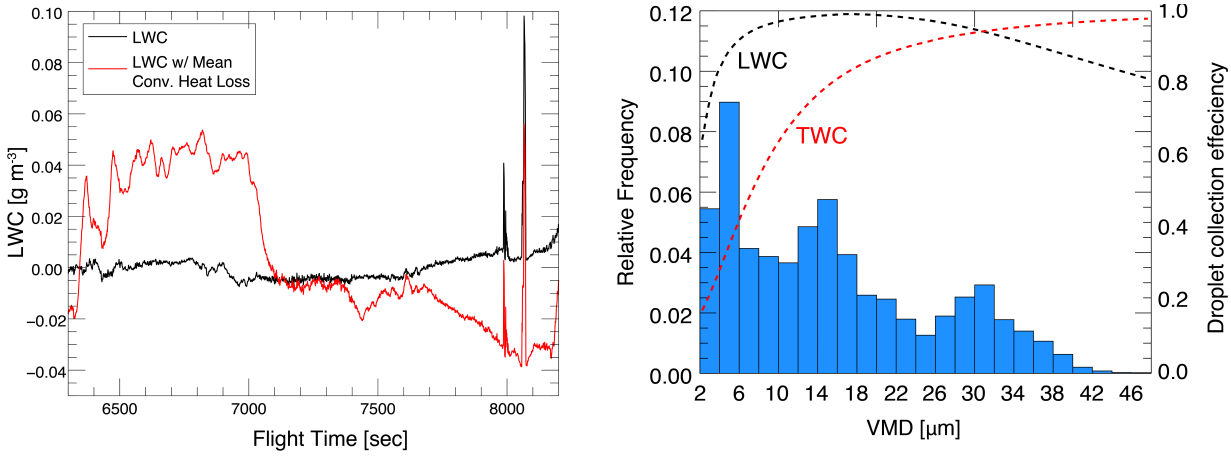

Figure 2. *(**a**) An example of baseline LWC drift (shown by the red line) that would be introduced by assuming a mean convective heat loss value (therefor neglecting convective heat loss airspeed and density dependence). The black line shows LWC calculated using a dynamic convective heat loss value. (**b**) CDP droplet size distribution binned by VMD for DSDs collected during COPE-MED. Dashed curves are estimates of droplet collection efficiencies for the LWC and TWC sensors (Korolev et al. 1998, Strapp et al. 2003, Schwarzenboeck et al. 2009).*

4. Objectives

A two-tiered methodology, including both laboratory-based experiments and in-situ analysis, will enhance the Atmospheric Science department's observational study abilities through improved error characterization for the CDP and Nevzorov devices. Proposed objectives fall into three general categories.

Firstly, a droplet generating calibration device will expand the department's ability to calibrate and characterize error sources for several optical cloud probes. Efforts are to be focused on preliminary system development, operating procedure development, and algorithm coding. The system will initially be capable of calibrating the CDP but future work will expand compatibility to include the FSSP and SPEC inc. 2D-S. Major objectives include

1) Hardware installation
2) Development of control software
3) Development of best operating practices
4) Conducting preliminary tests to confirm system performance
5) Collecting CDP calibration data including
    a) Position-dependent droplet sizing accuracy
    b) Sample volume dimensions

Objective 5 entails recording detailed measurements of CDP sample volume characteristics including position-dependent sizing accuracy and measurements of sample volume dimensions. CDP particle-by-particle data will provide detector pulse amplitudes for individual counting events; a parameter with much finer resolution than derived droplet diameters. Droplet generator results will be used to create a detailed map of sizing accuracy at locations throughout the CDP's sample volume (or "beam map". See figure 4b).

Secondly, algorithms will be developed to perform Nevzorov LWC and TWC calculations which consider well-defined error sources. Nevzorov algorithm focused objectives include:

6) Development of software to calculate Nevzorov LWC and TWC from UWKA data
    a) Algorithms will consider error sources including
        i) Estimates of droplet collection efficiencies from work by Korolev et al. (1998), Strapp et al. (2003), and Schwarzenboeck et al. (2009)
        ii) Corrections for convective heat losses which consider heat loss airspeed and density dependence (does not use a fixed approximation)
    b) Algorithms will accurately calculate baseline LWC and TWC without the need for manual corrections
7) Testing of algorithm performance using COPE-MED LWC calculations provided by Alexei Korolev

Thirdly, error assessment for the CDP and Nevzorov will be performed using in-situ data collected during the Precipitation and Cloud Measurements for Instrument Characterization and Evaluation (PACMICE) campaign. Investigations will utilize the two instrument's mutual LWC retrieval ability (a bulk measurement for the Nevzorov and DSD integration for the CDP) to characterize instrument performance. In-situ studies are to accomplish the following objectives:

8) CDP – characterize error including
    a) Mis-sizing due to sizing response error using
        i) Droplet generator calibration results
        ii) CDP/Nevzorov LWC comparison in low particle concentrations
    b) CDP LWC error due to coincidence events using
        i) Refined sizing response error estimates (objective 8a)
        ii) CDP/Nevzorov LWC comparison in all particle concentrations
9) Nevzorov – characterize potential error sources including
    a) TWC collection efficiencies for 25 – 50 μm VMD droplets using
        i) CDP/Nevzorov LWC comparison (incorporating results from objective 8)
        ii) Comparisons of LWC/TWC sensor liquid water content measurements
    b) Aircraft orientation effects using
        i) CDP/Nevzorov LWC comparison (incorporating results from objective 8)
        ii) Relationships of aircraft orientation and out of cloud Nevzorov LWC error

CDP mis-sizing specific investigations (objective 8a) are to be initially constrained to relatively low droplet concentrations in order to exclude error introduced by coincidence events. A threshold of relevant concentration ranges will be determined by considering droplet generator calibration data, CDP/Nevzorov LWC comparisons, and findings from previous studies by Lance et al. (2010, 2012).

Characterization of CDP LWC error contributed by coincidence events will be performed by considering the results of mis-sizing specific investigations (objective 8a) and CDP/ Nevzorov LWC agreement for all particle concentrations. It is expected that the occurrence of coincidence error will be evident as a positive correlation between particle concentration and absolute differences in CDP/Nevzorov LWC.

In-situ analysis will investigate two potential Nevzorov error sources; TWC sensor collection efficiencies for 25 – 50 μm VMD droplets and aircraft orientation effects. Work regarding TWC droplet collection efficiencies (objective 9a) will use CDP/Nevzorov LWC comparisons and comparisons of liquid water content measured by the Nevzorov's LWC and TWC sensors. The nature of aircraft orientation's affect on Nevzorov LWC error (objective 9b) will be evaluated using relationships of aircraft orientation/out of cloud LWC error and comparisons of Nevzorov/CDP LWC.

5. Development of a Water Droplet Generating Calibration System for Cloud Particle Probes

Designs for the water droplet generating calibration device are based on work by Nagel et. al. (2007), which was later expanded on by Lance et. al. (2010), in which a piezoelectric print head (typically used for circuit printing or biomedical applications) dispenses pure water droplets inside a tube containing a sheath airflow (MicroFab, inc.). The print head device includes a fluid cavity surrounded by a piezoelectric membrane which forces fluid through a precision glass nozzle. The piezoelectric element is driven by a programmable controller which supplies voltage pulses in order to create droplets at the nozzle's exit. Once created, the droplets are accelerated by the sheath flow, focused through the flow tube's tapered exit region, and passed through an instrument's sample volume. A high speed camera independently verifies droplet size, velocity, and trajectory while computer controlled microstages alter the point of sample volume injection. Generator setups can produce a range of droplet sizes, velocities, and concentrations by altering the position where droplet enter the sheath flow, interchanging print head size, and modifying print head driver pulses. Droplet generating calibration devices are especially adept at investigating an instrument's spatially-dependent sizing precision and measuring sample volume dimensions.

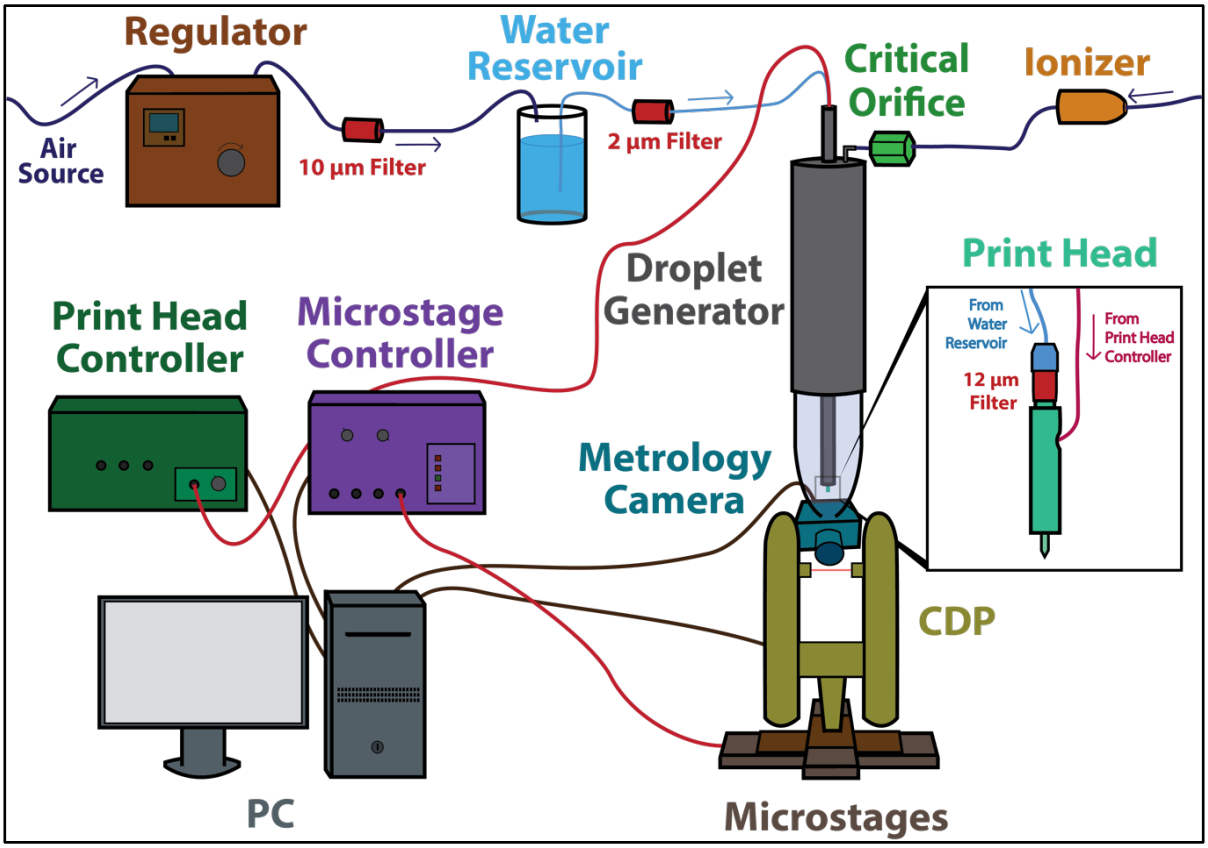

Figure 3. *Schematic of the droplet generator system layout. Note: brown lines are communication links to/from the PC, red lines are cables from controllers, purple denotes pressurized air lines, and blue shows water lines.*

Calibration system development is currently underway with a majority of components already installed and tested. Figure 3 shows a schematic of the major system components. The droplet generator assembly (in grey) includes a glass flow tube (semi-transparent structure at the bottom) and print head (available in diameters of 5 μm increments spanning 20 – 80 μm) positioned within the sheath flow. The print head device is fixed to the end of a movable rod. Raising or lowering the rod alters droplet in-flow residence time providing adjustment of droplet velocity and diameter (through evaporation).

Separate compressed air sources provide both reservoir water level regulation and sheath flow to the droplet generator assembly. A microfluidic pressure regulator placed between the first air source and reservoir provides both the precise adjustments required during print head operation and pass through of higher pressures used to purge water lines of air bubbles and contaminants. Control of sheath flow rate and minimization of flow tube/ambient pressure differential is accomplished using a critical orifice and choked flow principles.

Independent droplet diameter and velocity estimates are calculated using the glare technique, as initially described by Korolev et al. (1991). A high speed metrology camera images droplet glares (bright regions located at a droplet's left and right sides) as droplets are illuminated in the CDP's sample volume. Droplet diameters are estimated using glare pixel separation, pixel/distance relationships determined using glass microbeads, and camera geometry. Droplet velocity can be deduced by further considering a glare's Y-axis pixel counts and exposure times. Figure 4a shows an image of glares created by a 40 μm droplet.

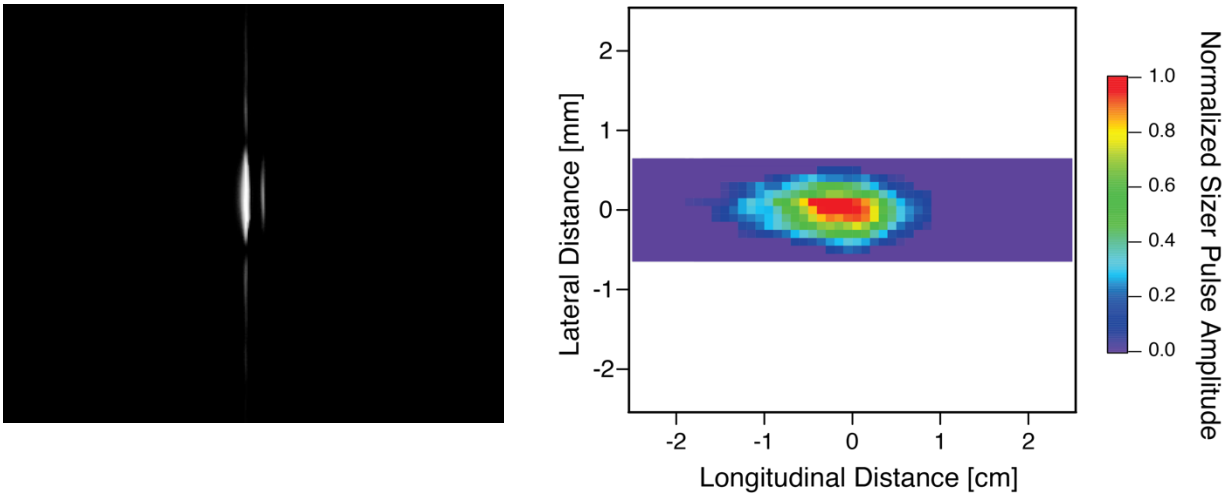

Figure 4. (a) *A 125 us exposure of 40 μm droplet glares captured during preliminary testing. (**b**) An example CDP beam map from work by Lance et al. (2012) which shows position-dependent sizing detector response.*

Reliable print head operation has proven to be problematic. The devices are intended to be operated in a cleanroom environment; a condition which cannot feasibly be met in

our lab. Therefor, clogging caused by both airborne particles and contaminants picked up by disconnected tubing is an ever-present issue. The addition of in-line filters on both the air and water supply lines (red cylinders in Figure 3) has decreased downtime due to blockages by a significant amount. But the need to clear print head clogs is still a common occurrence and procedures which utilize an ultrasonic cleaner, mild solvents, and a vacuum source for back flushing have been proven to be consistently affective. Achieving passage and ejection of droplets from the flow tube has also been arduous. Successful ejection is dependent on a precise combination of sheath flow rate, print head location, water reservoir pressure, and jetting parameter values. Static interactions between droplets and the flow tube often prevent successful droplet passage; an issue which has been remedied by placing an air ionizing device between the air source and droplet generator sheath flow inlet.

The microstage system remains as the last unintegrated component. A proposed system by ThorLabs, Inc. will allow droplet placement in the X/Y axes at sub-micron repeatability. Calibrations will be conducted by continuously operating the droplet generator while microstages reposition the CDP to cause droplets to traverse the sample volume in a serpentine pattern (where droplets are placed at set increments across the distance of the sample volume's Y-axis, move one increment in the X-axis, and traverse the Y-axis in the opposite direction). Both the microstage positioning and CDP data acquisition software incorporate LABVIEW which will allow the integration of microstage positioning and CDP sizing response data. CDP sizing and positioning data will be compiled to create a detailed parameterization of sizing performance or a "beam map" (see Figure 4b).

6. Nevzorov Data Processing

Nevzorov data processing routines have been developed (objective 6) and tested using well-established COPE-MED calculations (objective 7) provided by Alexi Korolev, an expert directly involved in Nevzorov development. Our calculated LWC and Korolev's independent values have been shown to be in good agreement despite using unique calculation methods. Algorithms include "dynamic" corrections for convective heat losses (heat loss values are based on parameterizations of airspeed and air density) and parameterizations of collection efficiency.

Algorithm processes require identification of clear air (out of cloud) points which is accomplished using the following methodology:

1) The ratio of LWC collector sensor voltage to LWC reference sensor voltage ($V_{ratio} = V_{lwc,col} / V_{lwc,ref}$) is calculated
2) A baseline V_{ratio} (or $V_{ratio,base}$) is defined by
   a) Dividing V_{ratio} into 30 second increments
   b) Locating each increment's minimum V_{ratio} value
   c) Applying a low pass filter to the selected minimum V_{ratio} values

3) A normalized voltage ratio is then calculated by taking the difference of voltage ratios and baseline voltage ratios ($V_{norm} = V_{ratio} – V_{ratio,base}$)
4) A threshold is set as the 25th percentile of V_{norm}
5) A preliminary subset of clear air points is selected where V_{norm} is less than the threshold value
6) The final clear air point subset is defined after excluding the largest 5% of preliminary V_{norm} values

Step 6 removes a small number of in-cloud points that are erroneously flagged as clear air. Figure 5a provides a graphic representation of the clear air filtering process. It should be noted that the process by no means flags every clear air point but it does provide a sample sufficient for subsequent calculations.

Nevzorov LWC is calculated using the following formulae as defined in the Nevzorov operating manual (Sky PhysTech, Inc.).

Sensor power consumption due to hydrometeor evaporation is calculated as

$$P_{lwc} = V_{col} * I_{col} - k * V_{ref} * I_{ref} \quad (1)$$

where V_{col} and V_{ref} are collector and reference sensor voltage and sensor current is denoted as I_{col} and I_{ref}. k is a convective heat loss coefficient (elaborated below).

Liquid water content is calculated as

$$LWC = \frac{P_{lwc}}{e * U * S * L^*} \quad (2)$$

e is particle collection efficiency (assumed to be 1 for these calculations), U represents true airspeed, S is collector sensor surface area, and L* is the heat expended for the vaporization of liquid water which is defined as

$$L^* = (T_{sensor} - T_{ambient}) * C_{liq} + L_V(T_{sensor}) \quad (3)$$

where $T_{ambient}$ is environmental temperature, C_{liq} is the liquid water specific heat capacity, and $L_{v\ liq}$ is the latent heat of vaporization at T_{sensor}.

The convective heat loss coefficient (k) is defined as a ratio of collector and reference sensor powers when points are measured in clear air environments.

$$k = \frac{V_{col} * I_{col}}{V_{ref} * I_{ref}} \quad (4)$$

k is dependent upon airspeed and atmospheric density. LWC calculations typically use mean k values which neglect these dependencies and can contribute to significant error. For example, using a mean k for our calculations would introduce LWC error on the order of 100% (assuming Korolev's COPE-MED calculations as truth). Our methods use a dynamic k value based on parameterizations of airspeed and density dependence which increases LWC confidence in low water content environments and negates the need for manual baseline corrections. Parameterizations require Nevzorov calibration maneuvers composed of out of cloud legs flown at various pressure levels and airspeeds. A March 2016 flight provided calibration data with the following attributes.

1) 4 legs flown at separate pressures
   a) 700 mb
   b) 600 mb
   c) 500 mb
   d) 400 mb
2) Each pressure level contained sections of 5 discrete indicated airspeeds spanning approximately 80 – 115 m s^{-1}
3) Calibration legs required
   a) Clear air
   b) Level flight
   c) Consistent airspeed within each discrete airspeed section

Parameterizations of k/airspeed relationships were calculated on a per-pressure level basis (one parameterization for each of the legs in bullet point 1) in order to investigate which calibration level was most suitable for future UWKA campaigns. Each of the pressure level legs were manually analyzed and five 60 second sections with discrete airspeeds were selected. Care was taken to exclude sections with significant pitch, roll, yaw, sideslip, or acceleration. An indicated airspeed vs. k exponential fit was applied to the datasets filtered from each of the flight level legs providing airspeed-dependent k estimates for P_{liq} calculations (equation 1). It should be noted that indicated, instead of true, airspeeds were employed because indicated airspeed includes an intrinsic "compensation" for differences in density.

Performance of each of the four airspeed/k parameterizations (where each parameterization was calculated from either 400, 500, 600, or 700 mb pressure level data) was tested using points sourced from subsequent UWKA flights. Flight data were filtered to select out of cloud test points using CDP concentration values. Points are considered out of cloud if CDP particle concentrations are less than 10 cm^{-3} for a consecutive 2 second period. The median absolute out of cloud LWC error (where LWC error is equal to LWC for out of cloud points) was used as a performance metric. The four parameterizations performed quite similarly but the 400 mb k parameterization showed the least absolute out of cloud LWC error with consistent performance across a

majority of indicated airspeeds. Therefor, calculations only use the 400 mb k parameterization. Figure 5b shows each parameterization's performance binned by test point indicated airspeed.

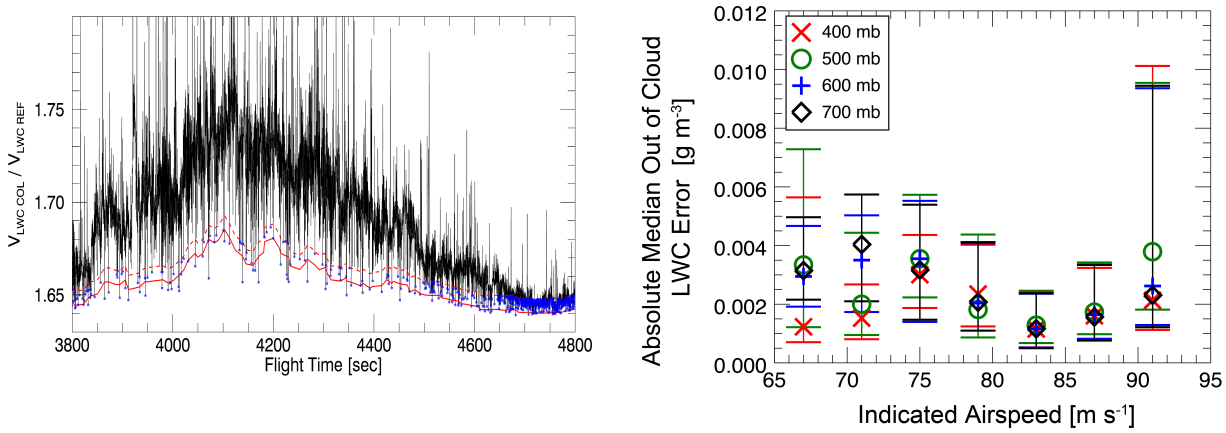

Figure 5. (a) *Shows a representation of the clear air selection process. Baseline values (red solid line) are minimum voltages from each 30 second period smoothed by a low pass filter. The threshold (red dashed line) is selected as the 25th percentile of normalized (*V_{norm}) voltage and points with normalized voltage less than the threshold are flagged as clear air (blue dots). ***(b)*** *Illustrates each k parameterization's performance. Out of cloud LWC error is considered to be LWC for out of cloud points. The 400 mb parameterization consistently showed the best performance across all mean indicated airspeed ranges (perhaps excluding the interval with 79 m s^{-1} mean indicated airspeed).*

LWC calculated with airspeed-corrected k values is still subject to error on the order of 0.03 g m^{-3} due to residual k density dependence. Correction for residual effects are performed by linearly fitting pressure vs. P_{liq} values for clear air data (where clear air data is selected using the process outlined at the beginning of this section) and then forcing the slope of the linear regression to zero. The aforementioned process typically reduces out of cloud LWC error caused by residual k density dependence by an order of magnitude.

LWC error could possibly be introduced by inaccurate measurements of environmental parameters but it was found that various sources of environmental data are so similar that resulting differences in LWC are trivial. The Nevzorov processing scripts use the following parameters; static pressure, static temperature, indicated airspeed, and true airspeed.

Approximately 130,000 COPE-MED data points were used to test the agreement of our calculated and Korolev's LWC values. The two sources were in very good agreement with a mean LWC difference (LWC - $LWC_{Korolev}$) of -0.0017 g m^{-3}. Figure 6a shows the median and interquartiles of percent LWC difference binned by Korolev's LWC. The first bin's comparatively large interquartile range could reasonably be caused by the smallness of that bin's LWC values. Korolev also performed manual baseline corrections for out of cloud periods whereas our methods didn't incorporate any corrections to compensate for baseline drift. Bins 2 - 8 have consistent interquartile

ranges and mean percent LWC differences very near -4.75%. It should also be noted that Korolev used a fixed approximation for L* instead of the more exact values (supplied by equation 3) used by our calculations. The Nevzorov operating manual states that such an approximation typically introduces LWC error on the order of 5%, making it reasonable to assume that much of the observed LWC difference is due to the usage of approximated versus more exact L* values (Sky PhysTech, Inc.).

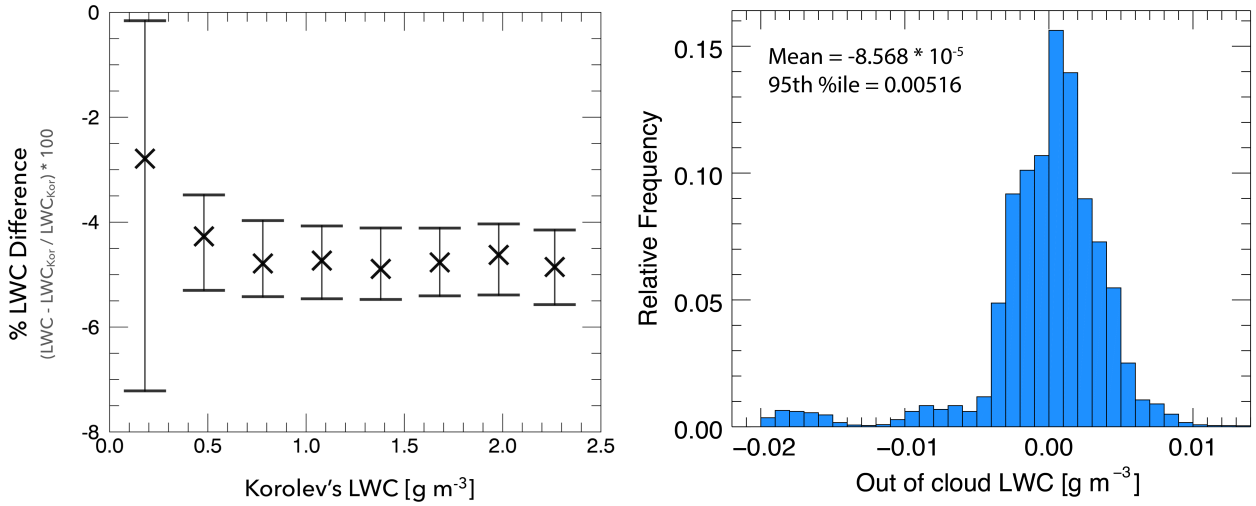

Figure 6. (a) *Median percent LWC difference and first and third quartiles of percent differences binned by Korolev's calculated LWC. A majority of the persistent ~4.75% LWC difference could reasonably be caused by differing methods of calculating L*.* ***(b)*** *LWC distribution for points filtered as clear air (based on CDP concentrations). The narrow distribution centered near 0.0 g m^{-3} suggests that LWC calculated with the newly-developed algorithms could have a baseline sensitivity less than 0.01 g m^{-3}.*

Our algorithm's baseline LWC accuracy was tested with a subset of out of cloud points (where out of cloud points must be 2 second periods with CDP concentrations of 10 cm^{-3} or less) collected during winter 2016 UWKA test flights. A histogram of out of cloud LWC (figure 6b) shows a fairly symmetric mode centered near 0.0 g m^{-3} and a much smaller secondary mode centered around -0.018 g m^{-3}. Overall, out of cloud points had LWC values slightly greater than the Nevzorov's estimated sensitivity of 0.003 g m^{-3} (Sky PhysTech, Inc.). Selected out of cloud points had a mean LWC of -8.568 * 10^{-5} g m^{-3} and a 95th percentile value of 0.00516 g m^{-3}.

7. In-situ Instrument Error Analysis

7.1 In-situ CDP Error Analysis

Data collected during the PACMICE campaign will provide a means to investigate error sources that potentially affect both the CDP and Nevzorov. CDP specific work will probe the nature of particle mis-sizing error contributed by non-ideal sizing response (objective

8a) and the nature of CDP LWC error contributed by coincidence events (objective 8b). Nevzorov specific investigations will characterized error contributed by non-unity TWC droplet collection efficiency (objective 9a) and aircraft orientation effects (objective 9b).

CDP mis-sizing error (objective 8a) will be investigated using PACMICE data and droplet generator calibration results. Investigations will focus on mis-sizing due solely to sizing response error and will therefor be constrained to relatively low CDP particle concentrations (in order to exclude mis-sizing error that is likely caused by coincidence events). Sizing response error is expected to be a systematic problem that will most likely contribute to well-behaved CDP/Nevzorov LWC biases. A combination of LWC bias analysis and droplet generator calibration results will provide a thorough characterization of CDP mis-sizing error.

Characterization of CDP LWC error caused by coincidence events (objective 8b) will be possible upon completion of mis-sizing error specific investigations. The relationship of CDP/Nevzorov LWC agreement and particle concentration will provide concentration dependent estimates of CDP LWC error. It is expected that coincidence errors will be much less prevalent than what was found in Lance et al.'s 2010 study because of the UWKA CDP's sizing detector pinhole mask. In fact, a 2012 follow-up study by Lance et al. found that such a pinhole mask reduced mis-counting error by 27% at concentrations of 500 cm^{-3}. Sulkis' 2016 analysis of COPE-MED data also found little evidence of significant coincidence error. More detailed analysis using refined error characterization, droplet generator results, and PACMICE data is nonetheless relevant especially when considering the potential magnitude of coincidence induced error.

Droplet collection efficiencies for both the Nevzorov's LWC and TWC sensors have been examined in several studies by Korolev et al. (1998), Strapp et al. (2003), and Schwarzenboeck et al. (2009). Cumulatively, the three studies provided collection efficiency estimates for droplets with VMD of 2 to well over 200 μm but TWC sensor efficiencies for 25 - 50 μm VMD droplets were perhaps the least explored. It is important to more completely understand TWC collection efficiencies in order to accurately discriminate between liquid water and ice in mixed phase clouds. CDP/Nevzorov LWC comparisons and refined CDP LWC error estimates will be used to test the truthfulness of TWC efficiency estimates provided by the aforementioned three studies (objective 9a). A second data source will be provided by comparisons of LWC/TWC liquid water content values and previously parameterized estimates of LWC collection efficiency.

The Nevzorov features a rotating vane designed to decrease error due to variations in aircraft pitch but it is suspected that aircraft orientation may still affect water content measurements. CDP/Nevzorov LWC comparison and out of cloud Nevzorov LWC error will help characterize various potential sources of orientation-related error (objective 9b). A preliminary analysis of COPE-MED data investigated possible error related to aircraft pitch, yaw, sideslip, roll, and presence of turbulence. No significant trends in aircraft orientation vs. out of cloud LWC error were detected but follow-up analysis of PACMICE data will provide confirmation that aircraft orientation is indeed a non-issue.

8. Timeline

- End of 2016 spring semester
  - Nevzorov uncertainty characterization completed for known sources
  - Nevzorov algorithm performance tested using COPE-MED data
- End of summer 2016
  - Majority of droplet generator components installed and tested
  - Best operational practices defined
- End 2016 fall semester
  - All droplet generator components installed and tested
  - Required operational software developed
  - Complete CDP calibration data collected
  - Initial PACMICE CDP/Nevzorov error investigations underway
- End of winter break 2016
  - CDP/Nevzorov uncertainty investigations nearing completion (using full fall/winter dataset)
  - Initial thesis writing stages underway
- Mid 2017 spring semester
  - PACMICE error investigations complete
  - Initial thesis draft complete
- End of 2017 spring semester
  - Thesis completed and successfully defended

9. References

Droplet Measurement Technologies, Inc., 2014: Cloud Droplet Probe (CDP-2). http://www.dropletmeasurement.com/products/airborne/CDP-2.

Gunn, R. and Kinzer, G. D., 1949: The terminal velocity of fall for water drops in stagnant air. *J. Meteor*. 6, 243-461

Jackson, R. C. et al., 2014: An assessment of the impact of antishattering tips and artifact removal techniques on cloud ice size distributions measured by the 2D cloud probe. *J. Atmos. Ocean. Technol.*, **31**, 2567–2590, doi:10.1175/JTECH-D-13-00239.1.

Korolev, A. V. et al., 2013: Improved airborne hot-wire measurements of ice water content in clouds. *J. Atmos. Ocean. Technol.*, **30**, 2121–2131, doi:10.1175/JTECH-D-13-00007.1.

Korolev, A. V. et al., 1998: The Nevzorov airborne hot-wire LWC-TWC probe: Principle of operation and performance characteristics. *J. Atmos. Ocean. Technol.*, **15**, 1495–1510, doi:10.1175/1520-0426(1998)015<1495:Tnahwl>2.0.Co;2.

Korolev, A. V. et al., 1991: Evaluation of measurements of particle size and sample area from optical array probes. *J. Atmos. Ocean. Technol.*, **8**, 514–522, doi:10.1175/1520-0426(1991)008<0514:EOMOPS>2.0.CO;2.

Lamb and Verlinde, 2011: Physics and Chemistry of Clouds. Cambridge University Press, 584 pp.

Lance, S. et al., 2012: Coincidence errors in a cloud droplet probe (CDP) and a cloud and aerosol spectrometer (CAS), and the improved performance of a modified CDP. *J. Atmos. Ocean. Technol.*, **29**, 1532–1541, doi:10.1175/JTECH-D-11-00208.1.

Lance, S. et al., 2010: Water droplet calibration of the Cloud Droplet Probe (CDP) and in-flight performance in liquid, ice and mixed-phase clouds during ARCPAC. Atmos. Meas. Tech., 3, 1683–1706, doi:10.5194/amt-3-1683-2010. http://www.atmos-meas-tech.net/3/1683/2010/.

MicroFab Inc.: Applications Overview. Accessed 9 August 2016. [Avalable online at http://www.microfab.com/overview-sp-1927588172]

Morrison, H., and J. A. Milbrandt, 2014: Parameterization of Cloud Microphysics Based on the Prediction of Bulk Ice Particle Properties. Part II: Case Study Comparisons with Observations and Other Schemes. J. Atmos. Sci., 72, 287–311, doi:10.1175/JAS-D-14-0065.1. http://journals.ametsoc.org/doi/abs/10.1175/JAS-D-14-0065.1.

Nagel, D. et al., 2007: Advancements in Techniques for Calibration and Characterization of In Situ Optical Particle Measuring Probes, and Applications to the FSSP-100 Probe, J. Atmos. Oceanic Technol., 24, 745–760, doi:10.1175/JTECH2006.1, 2007.

Perrin, T. et al., 1998: Modeling coincidence effects in the Fast-FSSP with a Monte Carlo model. *Preprints, Conf. on Cloud Physics, Amer. Meteor. Soc., Everett, WA*, 112–115.

Schwarzenboeck, A. et al., 2009: Response of the Nevzorov hot wire probe in clouds dominated by droplet conditions in the drizzle size range. *Atmos. Meas. Tech.*, **2**, 779–788, doi:10.5194/amt-2-779-2009. http://www.atmos-meas-tech.net/2/779/2009/.

Sky PhysTech, Inc.: Operating Manual, Nevzorov hot wire LWC / TWC Probe.

Strapp, J. W. et al., 2003: Wind tunnel measurements of the response of hot-wire liquid water content instruments to large droplets. *J. Atmos. Ocean. Technol.*, **20**, 791–806, doi:10.1175/1520-0426(2003)020<0791:WTMOTR>2.0.CO;2.

Sulkis, J., 2016: A Comparison and Survey of the Measured Cloud Liquid Water Content and an Analysis of the Bimodal Droplet Spectra Observed During the Summer 2014 Convective Precipitation Experiment – Microphysics and Entrainment Dependencies (COPE-MED) Field Campaign. University of Wyoming

Tölle, M. H., and S. K. Krueger, 2014: Effects of entrainment and mixing on droplet size distributions in warm cumulus clouds. J. Adv. Model. Earth Syst., 6, 281–299, doi: 10.1002/2012MS000209.